Framework for modal based assessment of liner structures

Karsten Knobloch*, Larisa Grizewski†, Fleming Kohlenberg‡, and Maximilian Behn‡
German Aerospace Center (DLR), 10623 Berlin, Germany

Julia Genßler§
DLR Institute of Electrified Aero Engines, 03046 Cottbus

A framework for the detailed investigation of the acoustic damping of higher order modes in an annular duct was set up and a first series of experiments was conducted investigating a noise absorbing section with homogeneous impedance and good sound absorbing performance, and a reference hard-wall section. The new setup enables the comparison of plane wave sound attenuation as obtained in small duct setups with measurements in the annular setup and in addition the acoustic damping of individual modes up to azimuthal mode order m=8 and radial mode order n=1. The paper addresses the investigation of the capabilities and limitations of excitation of individual dominant modes, of uncertainties of the setup and associated methods of data processing as well as the importance of losses in the acoustic boundary layer for the propagation of higher order modes.

I. Introduction

Acoustic liners - as used for instance in aero-engine inlets as passive noise reduction means - are still subject to intensive development and scientific investigations. While the basic operation principle is fairly well understood, the correct modelling of even single degree of freedom (SDOF) liners, their acoustic impedance, and finally the prediction of the expected noise attenuation for a specific application remains difficult and subject to high uncertainties due to effects of (high speed) grazing flows and non-linearities introduced by high sound pressure levels. The complexity (and uncertainty) of prediction increases further for liners with more degrees of freedom (2DOF/MDOF), and with actual installation effects from drainage slots and splices which introduce circumferential irregularities in the wall impedance seen by the complex sound field to be attenuated.

Prediction methods therefore often rely on empirical data and tests of liner sample structures, which yield validation data for novel liner structures - usually in the form of complex impedances (frequency-dependent resistance and reactance values). These tests are often confined to plane wave acoustic excitation in relatively small duct setups in order to simplify the test and evaluation procedure, and reduce cost and time. Only very few facilities (e.g. the NASA CDTR [1, 2], the MAINE facility at Le Mans [3], the facility at the Laboratoire Roberval of UTC [4]) are capable to investigate the performance of liner structures considering the more realistic scenario of higher order (circumferential and radial) modes, which are always present in larger ducts and annular ducts, specifically above aero-engine inlet and bypass liners, and for many other full-scale applications.

In the current investigation, a dedicated setup was used for the generation of individual dominant acoustic modes in an annular duct, which allows the detailed assessment of scattering coefficients and acoustic losses for liner structures on a mode-by-mode basis. The possibility to compare the results of the annular setup to measurements in a duct setup used extensively in the past for liner characterisation under grazing flow in acoustic plane wave regime will yield valuable insights into experimental procedures for more realistic and reliable liner sample investigations and predictions.

While the emphasis of this paper is on the description of the setup, the excitation and evaluation procedures and methods, a first application using a 200 mm Basotect® foam patch presents a good validation case and provides first insights into the transfer of plane wave results to the attenuation of higher order modes.

The paper will be structured as follows: Details about the measurement setup can be found in Section II, while the methods of mode generation and processing of microphone array data is described in section Section III. Section IV includes the presentation and discussion of the experimental results for the Basotect liner and a hard-wall reference

*Scientist, Dept. of Engine Acoustics, karsten.knobloch@dlr.de
†former PhD candidate, Dept. of Engine Acoustics, now: Deutsche Bahn AG
‡PhD candidate, Dept. of Engine Acoustics
§PhD candidate, Dept. of Turbomachinery Acoustics, TU Berlin

This is the author's version of the work that was accepted for publication in the proceedings of the 30th AIAA/CEAS Aeroacoustics Conference held in Rome, Italy in June 2024.
The final version was published in the proceedings of the conference as paper no. 2024-3298: https://arc.aiaa.org/doi/10.2514/6.2024-3298

section, which serves as a baseline for the assessment of the setup and quantifies the influence of viscothermal losses at the wall. Finally, a conclusion summarizes the findings in Section V.

II. Experimental setup

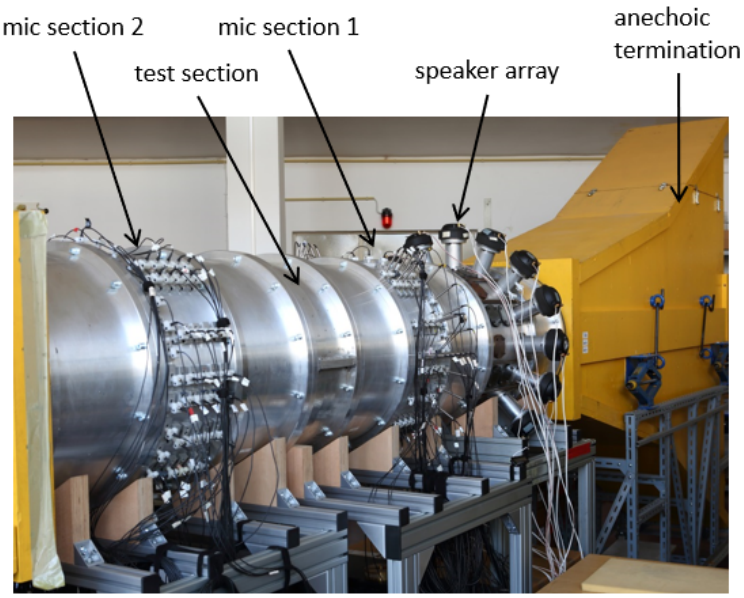

Fig. 1 MOSY setup for annular duct measurements including speaker array, two microphone sections and the test section with either hard-wall or liner barrel.

The general setup for mode synthesis and analysis was designed and applied earlier and is described extensively by Tapken [5–7]. It was also used by Gensch & Tapken [8] and Behn et al. [9] who created the software for synthesis, acquisition, and data processing. The so called 'MOSY' (mode synthesizer) facility is an annular duct with outer duct diameter of 500 mm and a center body of 330 mm diameter, which yields a channel height of 85 mm (see Fig. 1).

Anechoic terminations at both ends reduce end reflections for the setup when no grazing flow is present (fan stage removed from setup). The center body is supported by 13 slim steel rods to each end of the test section (i.e. they are not interfering with the sound field between the two microphone sections) and two additional steel rods required for support close to array 2 (the transmission side w.r.t. the test object). In the analysis of test results, there was no mode scattering observed in connection with these two rods. The overall length of the annular duct is about 2 m with hard-wall sections between microphone section 1 and test section, test section and microphone section 2, and finally microphone section 2 and the anechoic termination. This arrangement allows for additional decay of evanescent modes on impedance changes.

Two major cases were investigated: a hard-wall test section which should exhibit only marginal damping due to viscothermal losses in the acoustic boundary layer at the outer duct wall and the hub. This case serves as reference to verify the quality of the acoustic mode generation and analysis ('hard-wall case' for further discussion).

The second test object is a liner barrel composed of 100 mm thick Basotect® B foam which is mounted in a specific barrel flush with the outer duct wall with an axial extension of 200 mm (Fig. 2). The foam is neither axially nor in circumferential direction segmented and provides a homogeneous impedance on the outer duct wall ('liner case' for further discussion). In future investigations (not included in this paper), other liner structures - locally reacting or non-locally reacting will be tested with the same general setup.

There is the possibility to include a small fan in the overall setup - achieving a mean Mach number of about 0.07 in the annular duct. Results from tests with grazing flow are - for reasons of conciseness - not included in the paper.

An array of two rings of 16 speakers (BMS 4548) each was used which allowed for the individual generation of circumferential mode orders $m = \{-8 \ldots +8\}$ and radial mode order $n = \{0, 1\}$. This setup enables also the generation

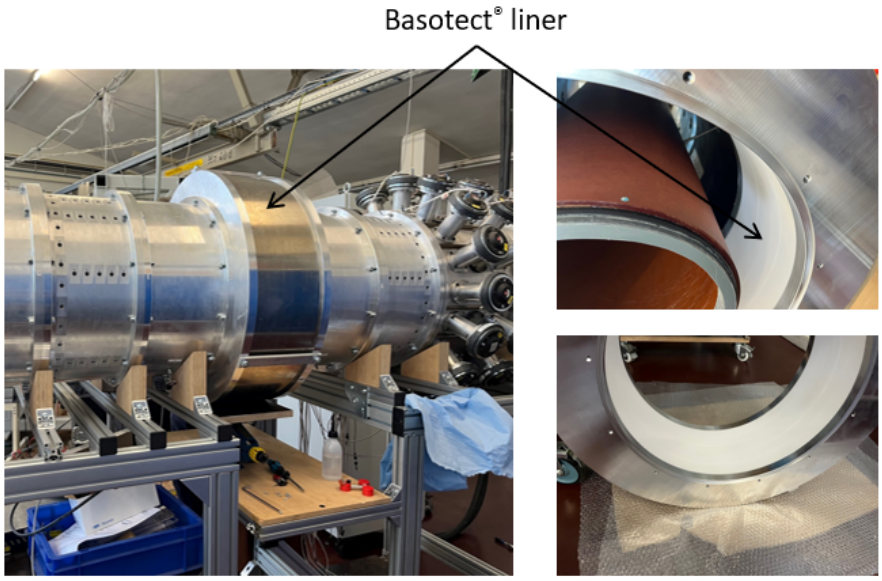

Fig. 2 Liner barrel with Basotect® B (white) patch. Left: mounted, right: view with mounted center body and without.

of higher azimuthal mode orders, but is not able to suppress all other modes in this case. If for example mode $m = 9$ is excited, at the same time mode $m = -7$ will be present with a significant amplitude (spatial aliasing).

The microphone arrays consist of 98 microphones (GRAS 40BP) each with a slightly asymmetric distribution over 7 rings at different axial locations (distance between first and last ring of an microphone array is 150 mm and roughly 1 m between the two arrays). Details on the microphone array design are given in [9]. The actual distribution was chosen after an analysis of desired acoustic modes and analysis capabilities. The range of cut-on mode orders is displayed in Fig. 3 up to 4.5 kHz.

The purely plane wave propagation - with no higher order modes able to propagate - is limited to frequencies below 270 Hz.

III. Mode Synthesis and Analysis

The sound field in annular ducts is described by radial modes which constitute the general solution of the Helmholtz equation [7]:

$$p(x, r, \phi) = \sum_{m=-\infty}^{+\infty} \sum_{n=0}^{+\infty} \left(A_{mn}^{+} \cdot e^{ik_{mn}^{+}x} + A_{mn}^{-} \cdot e^{ik_{mn}^{-}x} \right) \cdot f_{mn}(r) \cdot e^{im\phi}. \tag{1}$$

The radial modes are characterised by the mode amplitude A_{mn}^{+} and A_{mn}^{-} for modes propagating downstream and upstream, respectively. The spatial pressure distribution of each mode is determined by the radial mode shape factor $f_{mn}(r)$ given as a linear combination of Bessel functions, the axial wave number $k_{mn}^{\pm}$ and azimuthal mode order m. Figure 4 illustrates the pressure distribution exemplarily for the radial modes (-4,0) and (-4,1). In the no-flow case, the axial wave number is determined by

$$k_{mn}^{\pm} = \pm \alpha_{mn} k \tag{2}$$

with free-field wave number k and propagation factor $\alpha_{mn} = \sqrt{1 - \frac{\sigma_{mn}^2}{(kR)^2}}$. The (geometry-dependent) radial eigenvalue σ_{mn} is obtained from the hard-wall boundary conditions at the microphone sections.

The generation of individual radial modes can be achieved by the use of a speaker array. For the mode synthesis the amplitude and phase of each speaker are chosen such that the spatial pressure distribution of the target mode order is replicated. Various mode synthesis procedures have been developed in the past [10–12]. In this study, the technique presented by Tapken [6, 7] is applied, which is based on measured mode transfer functions of the individual speaker rings. While the speakers of the first ring are excited at the frequency of interest with a prescribed phase shift

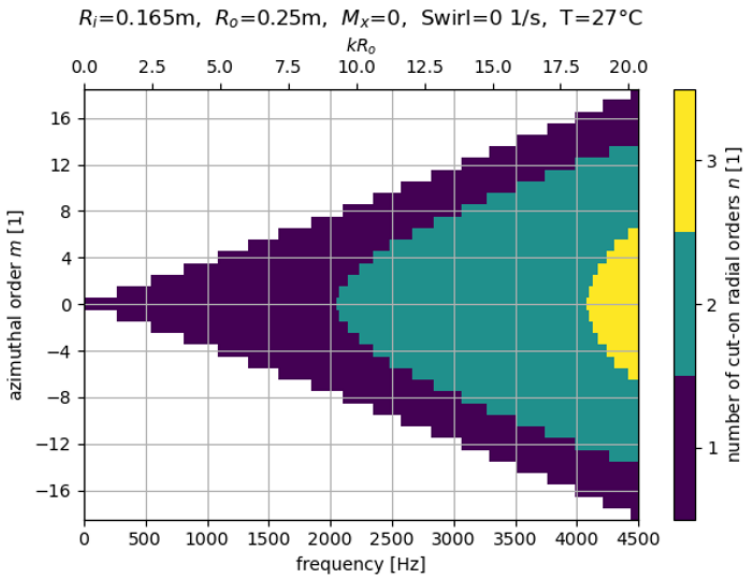

Fig. 3 Expected modes for MOSY setup (no flow case). With 16 speakers per speaker ring, $m = \pm 8$ is the maximum azimuthal mode order (with sufficient suppression of other modes) achievable.

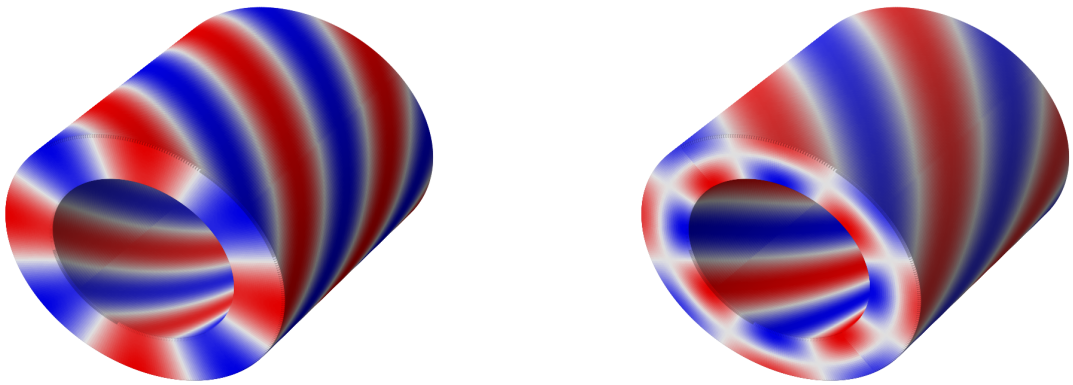

(a) (-4,0) (b) (-4,1)

Fig. 4 Spatial pressure distribution of radial modes (-4,0) and (-4,1)

$\exp(im\phi)$ depending on the target mode order m and circumferential speaker position, the sound field is measured by the microphone array at section 1 (see Fig. 1) to obtain the mode transfer function of the speaker ring. The procedure is then repeated for the second speaker ring. Subsequently, the gain factor for each speaker ring is computed by the following equation:

$$\mathbf{q} = \mathbf{H}_m^{\dagger} \cdot \mathbf{a}_m. \tag{3}$$

The vector $\mathbf{q} = [q_1, q_2]^T$ contains the gain factors. The transfer matrix $\mathbf{H}_m$ combines the measured mode transfer functions and the vector with the target mode amplitude $\mathbf{a}_m$. The dagger operator denotes the pseudo-inverse.

The sound field analysis is performed by Radial Mode Analysis [5] (RMA) on the sound pressure amplitudes measured by the microphone arrays at sections 1 and 2. The individual terms in Eq. (1) are considered as transfer functions from pressure measurements to mode amplitudes and combined in the RMA system matrix $\mathbf{W}$. Hence, the pressure amplitudes $\mathbf{p}$ measured at the respective microphone arrays are related to the mode amplitudes $\mathbf{a}$ by

$$\mathbf{p} = \mathbf{W} \cdot \mathbf{a}. \tag{4}$$

Typically, the solution of Eq. (4), i.e. the mode amplitude vector $\mathbf{a}$, is obtained by application of the pseudo-inverse $\mathbf{W}^{\dagger} = \left[\mathbf{W}^H \mathbf{W}\right]^{-1} \mathbf{W}^H$ which yields the least squares fit solution ('LSF'). The robustness of the LSF-solution can be evaluated on the basis of the relative accuracy of the mode amplitudes δA_m [5], which is presented in Fig. 5. The relative accuracy described the sensitivity of the mode amplitudes to disturbances in the sound pressure vector. For azimuthal mode orders, where only the first radial mode order $n = 0$ is cut-on, disturbances are suppressed and the determination of the mode amplitudes is robust. In the mode and frequency range with higher radial orders being cut-on the relative accuracy yields higher values indicating an increasing relative amplification of disturbances and related measurement uncertainties. Therefore, for the chosen microphone arrangement the frequency range for the standard Radial Mode Analysis using the least square fit is limited to about 2000 Hz.

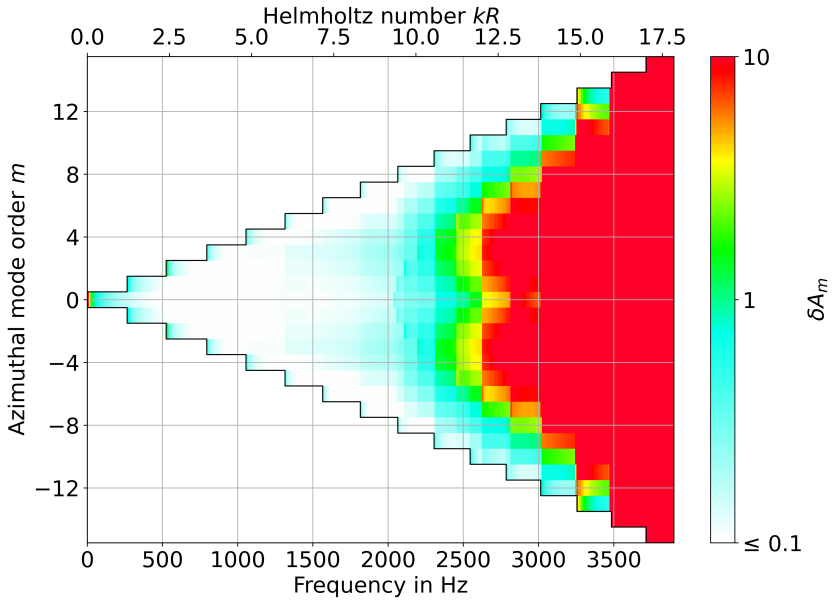

Fig. 5 Relative amplification of mode amplitudes for the least squares solution of Eq. (4)**.**

A possible means to extend the analyzable frequency range is the application of the BOMP algorithm (Block Orthogonal Matching Pursuit [13]) to solve Eq. (4) and to compute the mode amplitudes. The BOMP algorithm can overcome the limitations of the pseudo-inverse by exploiting sparsity of the mode spectrum [9, 14]. In our particular case, dominant modes of a single azimuthal mode order are generated by the loudspeaker array which manifests so-called block sparsity of all propagating radial modes with the target azimuthal mode order. Both, the loudspeaker array and the microphone arrays were utilized in combination with the BOMP algorithm for the investigation of mode propagation through stator vane rows in [9], where it was shown that reliable results can be obtained up to approx. 4 kHz. Based on this previous work, the overall frequency range for the current investigation was set to 500-3900 Hz.

IV. Results

In a first series of experiments, several test points (including for each test point two consecutive transfer measurements for the speaker rings and afterwards the actual mode excitation) were acquired using the LSF algorithm and target amplitude sound pressure level of 100 dB.

In a second series of experiments, the BOMP algorithm was used and sound pressure levels were set to 110 dB (in order to facilitate measurements with flow using the same setting afterwards).

Hence, a comparison of both algorithms can be included in the following presentation and discussion of results. Following aspects of the study are presented:

- Quality of single mode excitation and suppression of other modes
- Influence and assessment of losses at the wall
- Quality of measurement and data processing methodology by assessment of hard-wall case including frequency limit for procedure and comparison of LSF and BOMP algorithms
- Overall damping characteristics of the Basotect patch
- Dependency of acoustics damping on excited modes and frequency.

For the LSF algorithm, an uncertainty analysis could be made following the GUM guidelines. Assuming an uncertainty for microphone readings of 2% and static temperature uncertainty of 0.5 K, the error bars are compute for mode amplitudes and derived quantities for 2σ confidence interval. As will be seen later, this estimate accounts for random and (unknown) systematic errors, but does not fully characterize the accuracy and precision of the investigation. For the BOMP algorithm, a similar approach is not as straightforward as for the LSF and is currently not implemented. Therefore, BOMP results are given without error bars.

A. Hard-wall investigation - quality of mode excitation, attenuation at the wall, error analysis

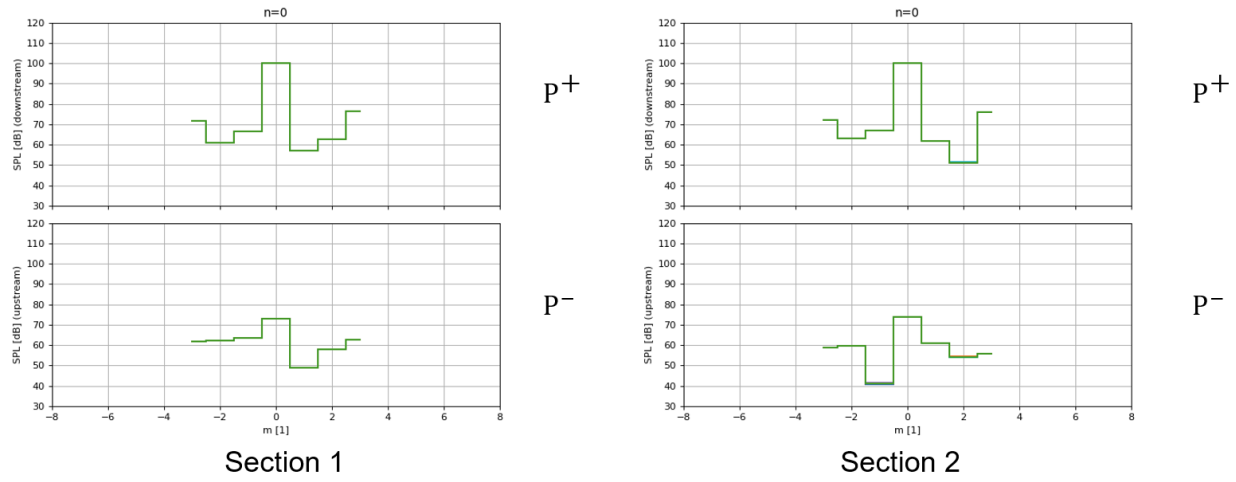

Fig. 6 Excitation of mode m=0 at 1000 Hz, showing the quality of suppression of higher order azimuthal modes by more than 20 dB, LSF algorithm.

Fig. 6 illustrates the excitation of the plane wave mode $m = 0$ for a frequency of 1000 Hz aiming for a target mode amplitude of 100 dB. The mode amplitudes in positive direction P^+ in (microphone) section 1 and 2 are for $m = 0$ almost exactly 100 dB. Between section 1 and section 2 is a hard-wall casing mounted with the same length as the liner barrel used later in this study.

As anticipated, there is no significant damping of the considered target mode (Fig. 6). All other modes which are able to propagate at this frequency are ($m = -3 \ldots + 3$) are suppressed by at least 20 dB.

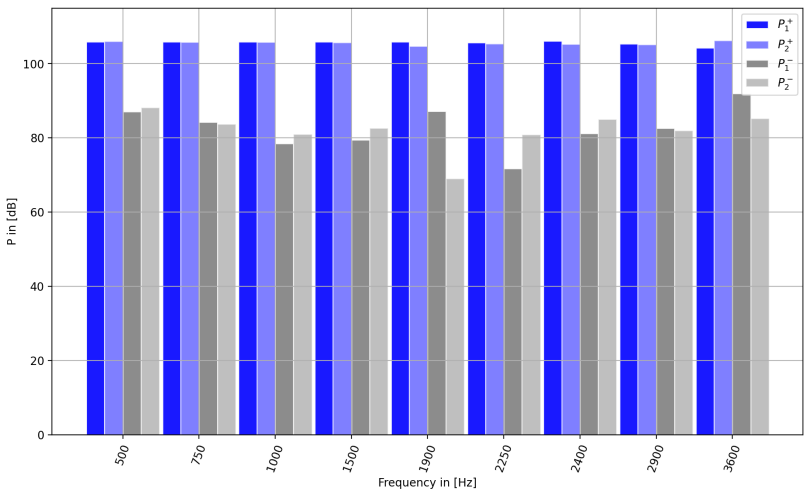

Fig. 7 Excitation of modes m=0 for various frequencies as measured before (section 1 = reflection side) and after (mic section 2 = transmission side) the hard-wall section, BOMP algorithm.

Excitation and measurement works equally well for almost all test point over the investigated frequency range between 500 and 3600 Hz (BOMP). For the hard-wall case, shown in Fig. 7, only the value at 3600 Hz suggesting a slight 'sound production' is obviously in error. It has to be kept in mind that mode (0,0) is rather difficult to generate and to measure due the necessary accuracy of microphone measurements (detecting the propagation of this mode with very little variations in microphone SPLs in axial direction and ideally no variation in circumferential direction) and the possible occurrence of very small and large amplification values at the same time for different speakers in order to generate mode $(0, 0)$ and suppress mode $(0, 1)$ (see Tapken [7]).

For the LSF algorithm (plot not shown), only frequencies between 500 and 2000 Hz were investigated for the hard-wall setup, with significant reduction of P_2^+ for 2000 Hz, which was suggested already by the plot of relative amplifications of mode amplitudes reaching value of unity around 2000 Hz (see Fig. 5).

A more detailed assessment of the ratio of the desired mode amplitude and the amplitude of the next most dominant mode for the BOMP test points is provided in the following scatter plot Fig. 8.

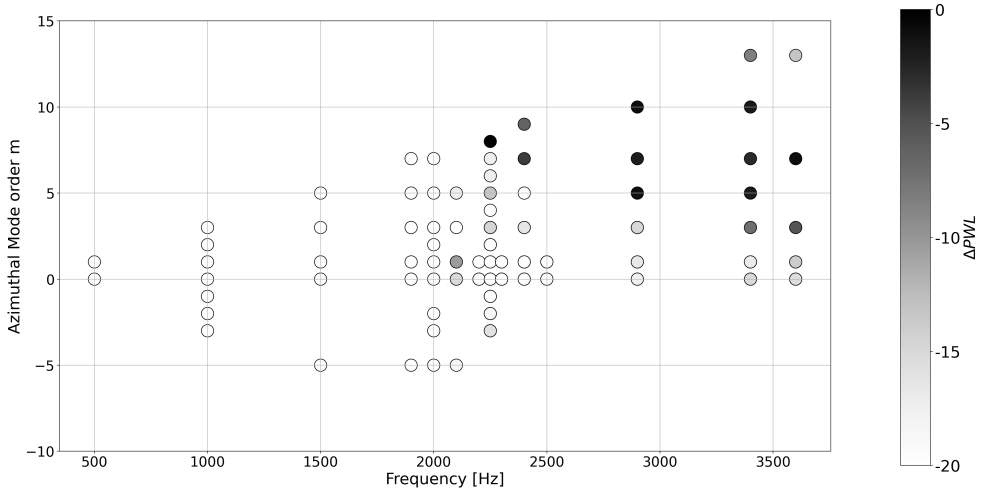

Fig. 8 Difference between dominant mode (here always the generated mode) and the second strongest mode on the reflection side of the test object, liner test case, BOMP algorithm, radial mode order n=0.

As expected, also the BOMP algorithm is limited by the specific arrangement of microphones and speakers, showing good results for most modes at frequencies below 3400 Hz with only exceptions for high mode orders which are caused

by the limited number of speakers, e.g. modes $m = -8$ and $m = 8$ excited at about the same amplitude for 2250 Hz.

In Fig. 9, the scattering coefficients, namely the reflection coefficient R_{mn}, the transmission coefficient T_{mn}, and the derived quantity dissipation Δ_{mn} for radial mode $(m = 0, n = 0)$ are plotted. The determination of the dissipation Δ_{mn} is done via an energy balance:

$$R^{\pm}_{mn} + T^{\pm}_{mn} + \Delta^{\pm}_{mn} = 1 \tag{5}$$

For the no-flow case, the dissipation reduces to

$$\Delta^{\pm}_{mn} = 1 - \left(\alpha_{mn} \left|r^{\pm}_{mn}\right|^2 + \alpha_{mn} \left|t^{\pm}_{mn}\right|^2\right) \tag{6}$$

R_{mn} and T_{mn} are the power quantities of the reflection and transmission coefficients, while r_{mn} and t_{mn} are the (modal) pressure quantities.

The dissipation is a good way to characterize different liner structures - and compare them if used in the (geometrical) identical setup. Here, the scattering coefficients provide an estimate of the quality of the whole framework, as it includes the target mode generation, the suppression of other modes, and the data acquisition by the microphones and its processing. If acoustic energy would leak into different modes not considered during the processing of single mode data, or the mode analysis procedure would not work well, we would see significant deviations from zero dissipation, which is the expected value for the hard-wall case.

In fact, Fig. 9, exhibits only marginal reflections for all modes (consecutively) excited and also very low transmission losses visible in coefficient T for modes $m = -3...2$. Please note that mode $m = 3$ was not excited/measured as we assume symmetry for positive and negative modes in this setup without any grazing flow and disturbances in the annular duct.

On the right hand side of the figure, the measured transmission loss (derived from the same data set) is plotted and found to be below 0.5 dB for all modes measured at 1000 Hz. The transmission loss data is compared to a model by Weng [15, 16] which considers the viscothermal losses at the duct wall.

Wengs model reduces to the same formulation as earlier models provided by Kirchhoff [17] and Beatty [18] for the no flow case, but includes convection effects for cases with flow in a more robust and accurate way than other models. However, effects of conversion of acoustic energy by turbulence and refraction of acoustic energy by shear layers are not included in his model. The “wide duct” assumptions Wengs model is based on, e.g. the thin acoustic boundary layers, are well satisfied for the current setup.

The model and the measured data fit very well - giving confidence in the reliability and suitability of the whole framework for liner assessment. Further, it can be concluded, that for short duct sections as used in the current setup, the viscothermal losses at the wall will be small compared to expected attenuation of specific liner patches.

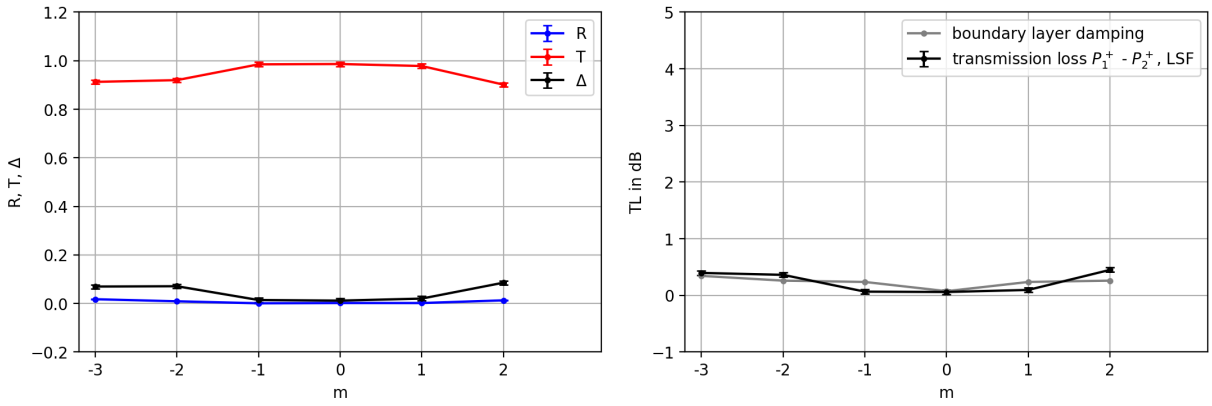

Fig. 9 Scattering Coefficients R, T, Δ as obtained by LSF algorithm for hard-wall measurements and different modes excited at 1000Hz (left) and comparison of measured transmission loss with prediction of losses according to Weng (right).
Note: Lines are introduced for better trend visibility and meaningless due to discrete modes orders

For the BOMP algorithm, scattering coefficients R, T, Δ and transmission loss TL are shown in Fig. 10 over frequency for mode $m = 0, n = 0$. The LSF algorithm yields similar results for test points up to 1500 Hz (not shown). However, for

test points at frequencies 1900 Hz, 2250 Hz, and 2400 Hz, there are deviations in transmission coefficient T and derived quantity Δ visible (reflection R remains unaffected). Looking at the transmission loss data in the adjacent plot, the values at those frequencies are off by at maximum 1 dB from expected (nearly) zero transmission loss. This highlights again the sensitivity of scattering coefficients R, T, Δ to the accuracy of measurements.

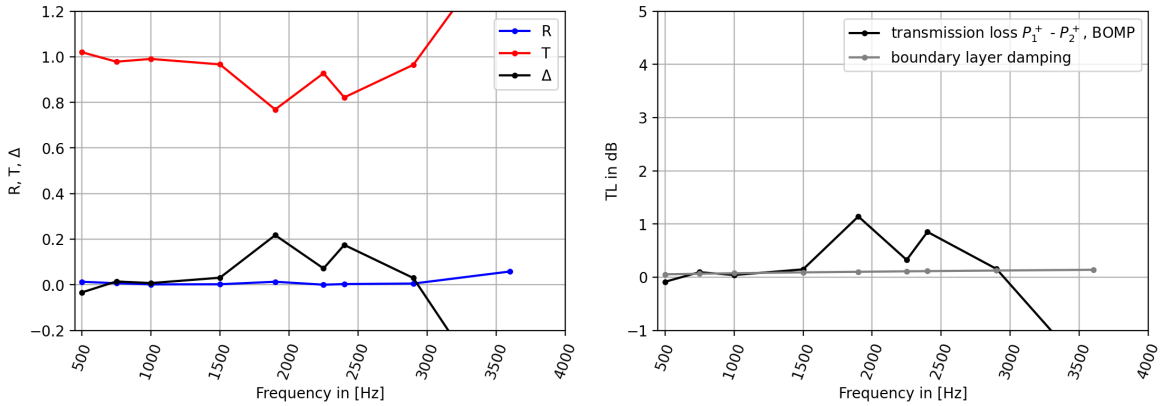

Fig. 10 Scattering Coefficients R, T, Δ for hard-wall measurements for mode (m,n)=(0,0), BOMP algorithm (left) and comparison of measured transmission loss with prediction of losses according to Weng (right).

For the investigation of the root cause of these deviations from expected "very low loss" behaviour, the list of cut-on frequencies for this annular duct setup reveals a certain number of modes that are close to their cut-on in this region (see Table 1). For a temperature of 21°C, following cut-on frequencies are in this region:

Table 1 Cut-on frequencies for MOSY setup at 21°C (294K) for several modes in the range of 1800-2400 Hz

Cut-on frequency [Hz]	1818	2035	2054	2066	2109	2197	2310	2316
Mode order (m,n)	(7,0)	(0,1)	(1,1)	(8,0)	(2,1)	(3,1)	(9,0)	(4,1)

Instead of the propagation factor α_{mn} (introduced above), the cut-on-ratio COR, is also widely used, which denotes for the no-flow case:

$$COR = \sqrt{\frac{1}{1-\alpha_{mn}^2}} \tag{7}$$

A cut-on-ratio below unity implicates an exponentially-damped non-propagating mode, while values above unity represent propagating modes. Values just above unity are connected to very poorly propagating waves with their wave fronts almost parallel to the duct axis which do not transport acoustic energy to a significant extent.

Further, one can calculate the axial propagation angle $\Theta_{mn}^{\pm}$ (i.e. the angle of the mode wave front with respect to the duct axis) according to Rice and Heidmann [19], which is in the no-flow case related to α_{mn} by:

$$\cos\Theta_{mn}^{\pm} = k_{mn}^{\pm}/k = \pm\alpha_{mn} \tag{8}$$

This large number of modes close to their cut-on implies mainly difficulties for the mode analysis with small axial wave numbers for several modes at the same time. As the mode excitation also depends on the accuracy of the mode analysis, there might be also a further small influence by the mode excitation respectively the suppression of unwanted modes at the same time. It is worth to note, that even modes which are very close but still below their cut-on frequency are evanescent, but only weakly damped if frequency is sufficiently low - thereby also adding to the complex sound field which needs to be analyzed at desired frequencies. As it visible from the list above, this detrimental effects can be expected largest for test points at 2000 Hz but also significant for 2250 and 2400 Hz.

The test point at 3600 Hz exhibits a transmission "gain" ($T > 1$) which was already visible in Fig. 7 and yields consequently a dissipation below zero, with reflection again almost unaffected. This frequency marks the upper limit for the analysis of at least the (very sensitive) hard-wall case.

Finally, the transmission loss as determined from measurements with BOMP algorithm for those frequencies in the "dense cut-on-region" are shown in Fig. 11 versus the excited mode order and are compared to the predicted thermoviscous losses. For the measurements at 1500 Hz (upper left), agreement is very good.

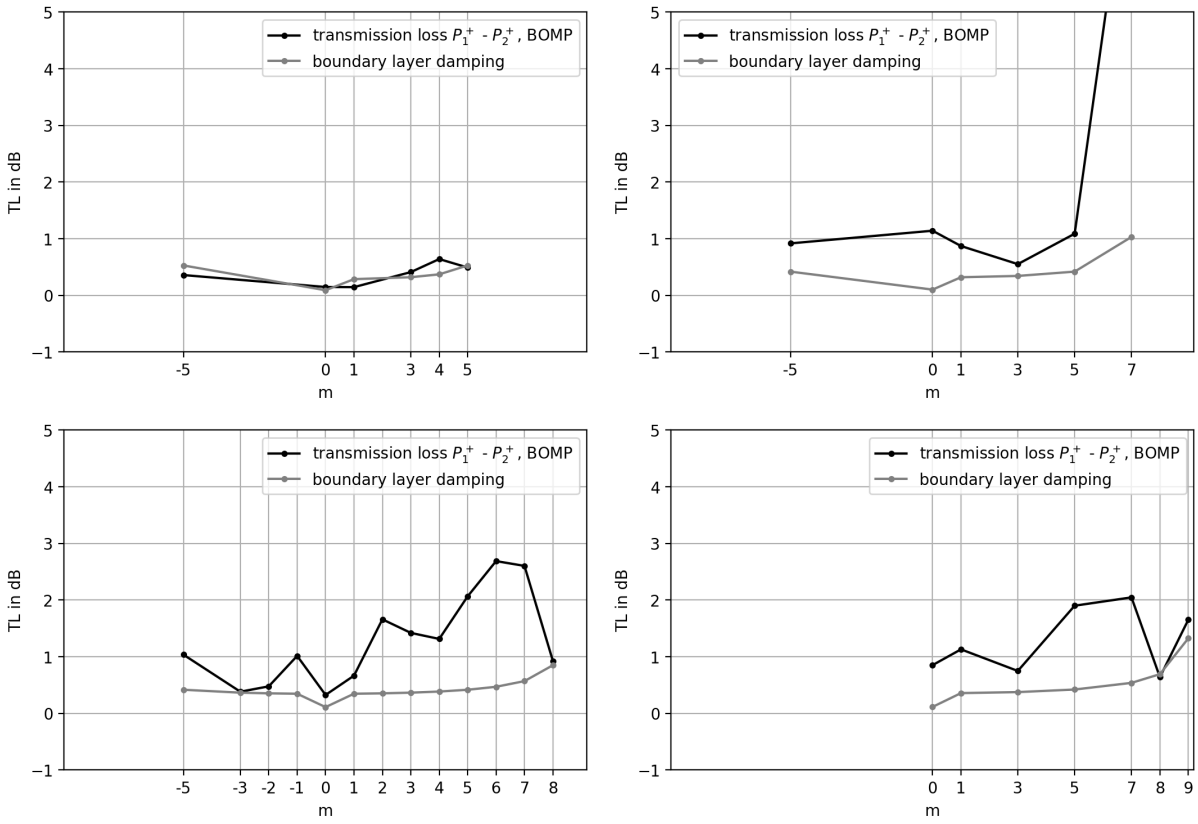

Fig. 11 Comparison of measured transmission loss with prediction of losses according to Weng for 1500 Hz, 1900 Hz (upper left and right), 2250 Hz and 2400 Hz(lower left and right). BOMP algorithm, $n = 0$. Deviations from expected thermo-viscous losses occur due to the cut-on of several other modes between 2000 and 2300 Hz, but are in most cases still rather small compared to usual liner attenuation.

For the other frequencies (e.g. 1900 Hz in the upper right), deviations are smaller for low azimuthal mode orders with mode $(7, 0)$ having the largest deviation - which could be attributed to the mode being just above its cut-on limit (1818 Hz) and is therefore propagating only very slowly in axial direction. There is no clear tendency for the remaining data points with respect to their deviation from prediction loss values with some of the higher mode orders being closer to the prediction than others. Care must be taken to check for every single measurement the ratio of excited mode amplitude to next highest dominant mode, cut-on ratio (or interchangeably: propagation angles) and density of cut-on modes in the vicinity of the considered frequency.

Nevertheless, the presented measurement results show an impressive range of frequencies and mode orders, which can be excited with sufficient dominance above other modes and measured accurately with the two microphone arrays.

B. Liner test case - scattering coefficients for plane wave and higher order modes

In order to investigate the attenuation of various acoustic modes by different liner structures, an interchangeable test section is placed between the two microphone segments. As the first test case, a homogeneous patch of foam was chosen, that is expected to provide a significant noise attenuation over a large frequency range down to low frequencies

due to its thickness of 100 mm. The axial length of 200 mm represents an L/D ratio of 0.4.

In Fig. 12, the scattering coefficients and transmission for the lined section are given for the plane wave mode $m = 0$ as determined by the LSF algorithm (upper left). The data points around 2000 Hz and at 2250 Hz could be probably omitted as they are expected to be biased by strong amplifications of uncertainties (compare Fig. 5). However, comparing with the upper right plot, the results for the BOMP show similar trends. Nevertheless, the physically unlikely scatter in the data in the marked regions - was observed to a comparable extent for the hard-wall case (Fig. 10) too, and is expected to be caused by the cut-on of several modes. In any case, the values still allow to obtain a certain decreasing trend for the dissipation and the respective transmission loss (lower left plot). For frequencies above 2500Hz, the data is likely less impacted by the limitations of mode decomposition and exhibits a further decreasing attenuation of the plane wave mode $(0, 0)$. Just above 2000 Hz, the first radial mode order for $m = 0$, i.e. mode $(0, 1)$ is able to propagate ("cut-on"), which experiences a stronger attenuation than mode $(0, 0)$ (lower left). However, it should be remembered that the result shown for mode $(0, 1)$ is not a "spill-over" from mode $(0, 0)$, but is explicitly excited and measured.

Overall, the results indicate a rather good and constant dissipation of acoustic energy, visible in the dissipation coefficient $\Delta \approx 0.8$ and a transmission loss of 7-9 dB over the entire range between 500 and about 1900 Hz, with a decreasing trend for higher frequencies. The losses at an equally long hard wall section, estimated as before with the Weng model, are negligible compared to the losses generated by the 200 mm Basotect foam patch.

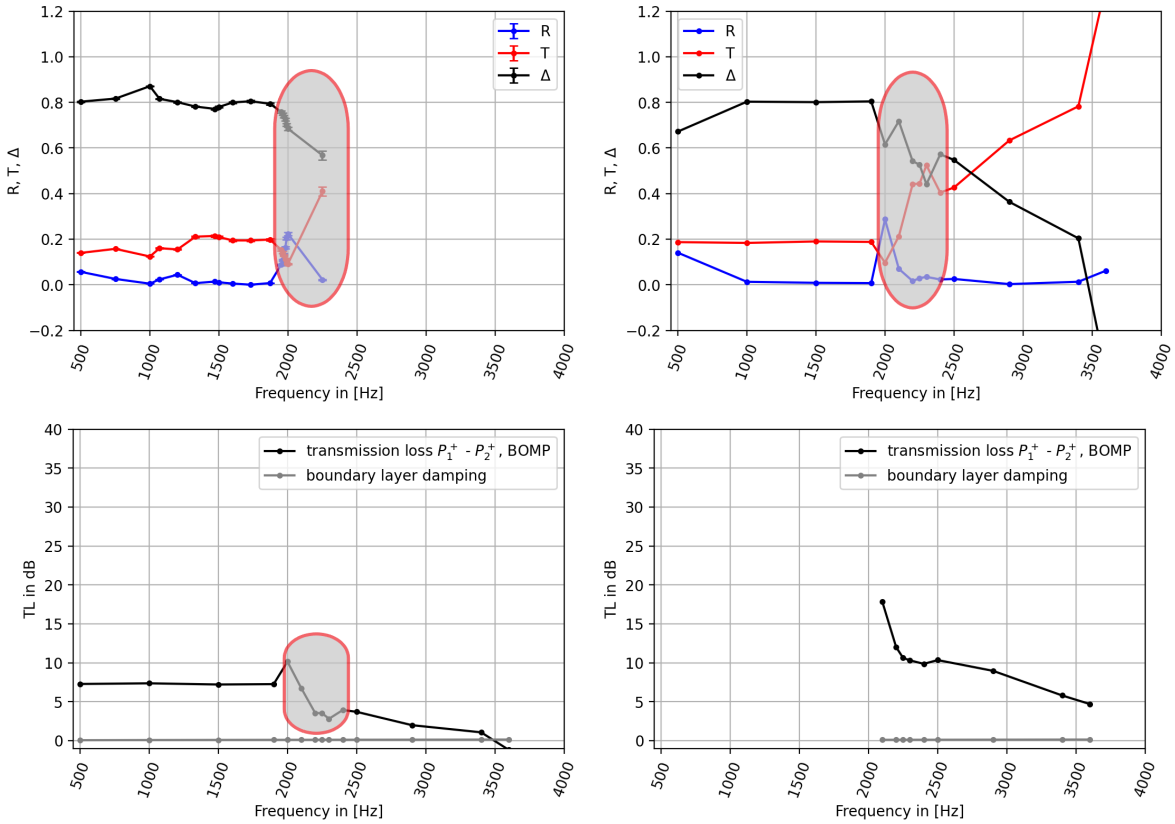

Fig. 12 Scattering Coefficients R, T, Δ for liner measurements for various frequency and plane wave $m = 0$ (left: LSF and right: BOMP with "dense-cut-on-region" marked, both n=0) and comparison of measured transmission loss with prediction of losses according to Weng (both BOMP,lower left n=0, right n=1).

In Fig. 13, the scattering coefficients and transmission loss are plotted for the attenuation of mode $m = 4$ shown over frequency (LSF algorithm). Below a frequency limit of about 1050 Hz, the mode $m = 4$ is not able to propagate in the duct (is an evanescent mode). Several data points were taken near the cut-on frequency of this point with the results supporting the general conclusion, that modes near their cut-on frequency are very difficult to generate and to measure with large uncertainty of data. The third plot (lower right) shows the same data as the one on the lower left, but using the cut-on ratio COR instead of the frequency for the abscissa. However, what is also observable from Fig. 13, in

particular from the transmission loss on the right hand side plot, is the increased transmission loss due to the spiraling mode with only slow propagation in axial direction.Thereby, the mode has more interactions with the lined section, leading consequently to a stronger dissipation of acoustic energy. The data point closest to cut-on (1065 Hz) has a $COR = 1.0014$ and an angle $\Theta_{4,0}$ to the duct axis of 87.8°. For frequencies well above the cut-on, the transmission loss converges to about 11 dB with a corresponding dissipation of about 0.9.

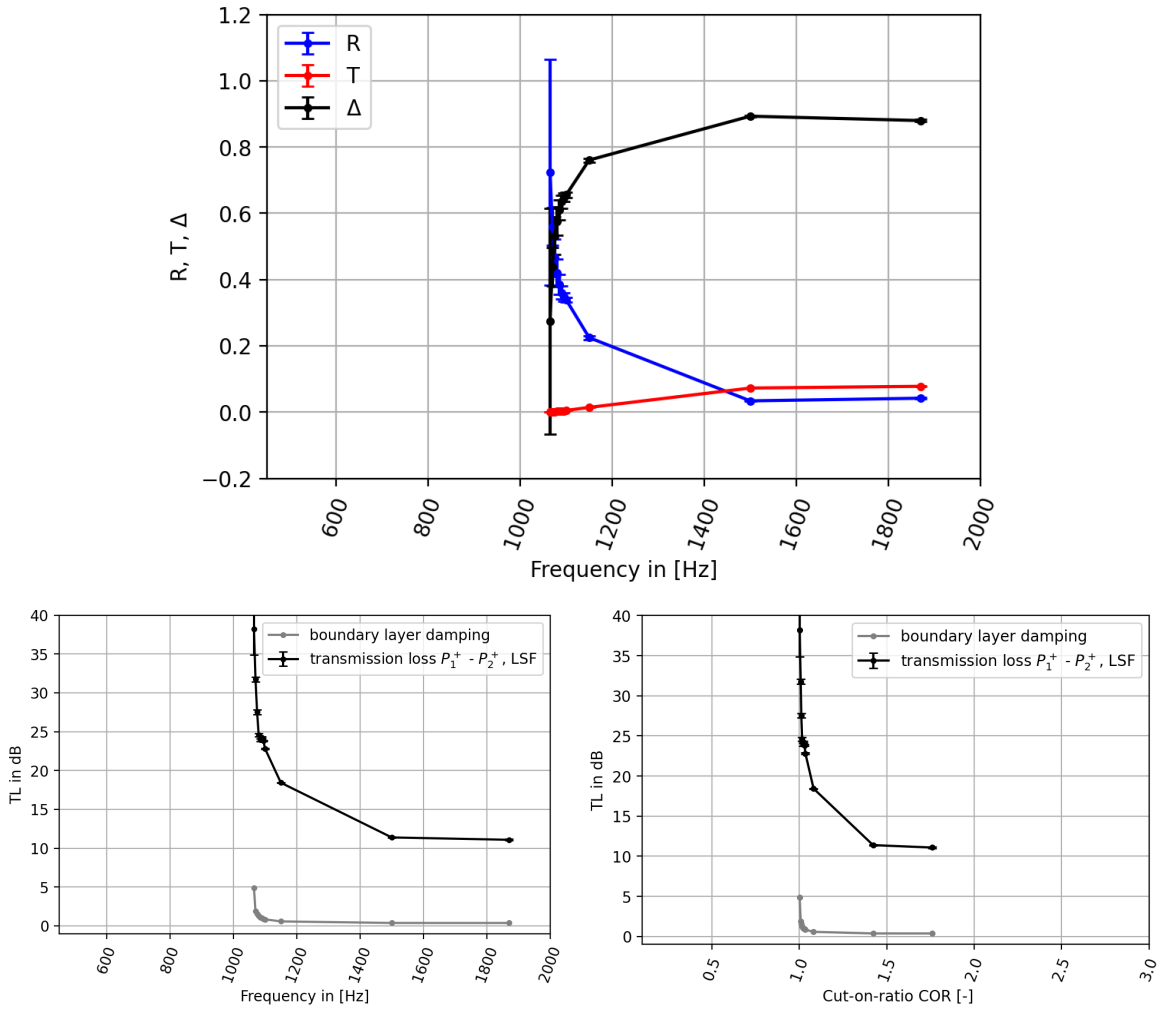

Fig. 13 Scattering Coefficients R, T, Δ for liner measurements for various frequency and azimuthal mode $m = 4$ (upper), which has its cut-on frequency at about 1050 Hz and comparison of measured transmission loss with prediction of losses according to Weng (left: versus frequency, right: versus cut-on-ratio COR).

Near cut-on conditions were explored in the context of effective noise suppression already by Heidelberg [20] and co-workers relating the achievable attenuation (transmission loss) directly to the cut-on-ratio. They predicted attenuation of up to 200 dB if just close enough to the actual cut-on. As this tremendous effect is tied to a very narrow frequency range, it will be very likely not be of practical interest for modern aero-engine liners with desired broad-band characteristics.

In Fig. 14 and 15, the scattering coefficients and transmission loss are plotted for frequencies of 1000 Hz and 1500 Hz, respectively, for the modes able to propagate for this frequencies (again, some modes are omitted due to expected symmetry). Fig. 14 includes again a comparison between LSF (upper row) and BOMP (lower row), while Fig. 15 shows only the scattering data for LSF (left) and BOMP (right).

Overall, data are in fairly good agreement, with the BOMP data expected to be more reliable when observing the improved symmetry for positive and negative mode orders, which can be expected when no grazing flow or other

disturbances are present. In general, the transmission loss shows an increasing tendency for higher mode orders (positive and negative), which is again attributed to the propagation angle of the modes. The reduction in transmission for higher mode orders coincides with a slight increase of reflection for these modes, which in turn yields only small changes to the dissipation Δ.

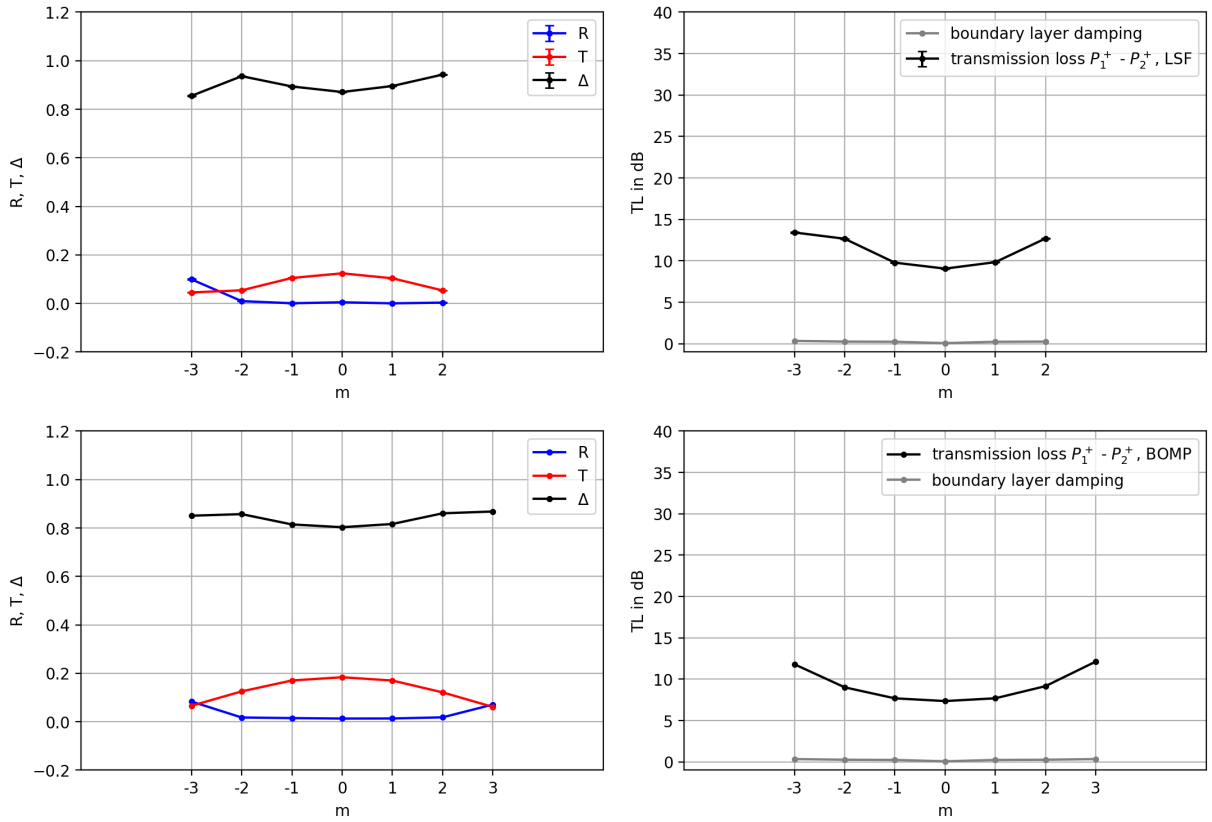

Fig. 14 Scattering Coefficients R, T, Δ for liner measurements and different modes excited at 1000Hz (left) and comparison of measured transmission loss with prediction of losses according to Weng (right). Upper two graphs for LSF, lower two for BOMP algorithm displaying further improvements of already good results.

From both plots it can be derived, that the plane wave mode $m = 0$ is the least attenuated mode, with an increase from 7 dB ($m = 0$) to about 18 dB ($m = 5$) in transmission loss for the 1500 Hz case.

C. Measurements with flow

Some measurements in the series of experiments have been made with a certain grazing flow above the liner. A fan with very simple blades was mounted to the end of the test rig, behind the anechoic termination of section 2. By operating it in the one or the other rotation direction, it was possible to suck the air through the test-rig (the positive direction in terms of acoustics) or blow it through the test rig (negative direction). Due to the very simple blade shape, low electric power, and poor transition from duct to fan hub, the flow speed as measured by a Prandtl-tube is limited to Ma=0.07 in both cases.

In order to concentrate on the general setup and measurement procedure, cases with flow are not presented in this paper. Further it is assumed, that convective effects, influencing the liner attenuation, are comparably small at these Mach numbers as vast experience from test in other facilities of the group showed in past investigations.

Nevertheless, measurement procedure and algorithms are suited also for investigations with grazing flow - which opens up further options when using other driving units than in the current test campaign.

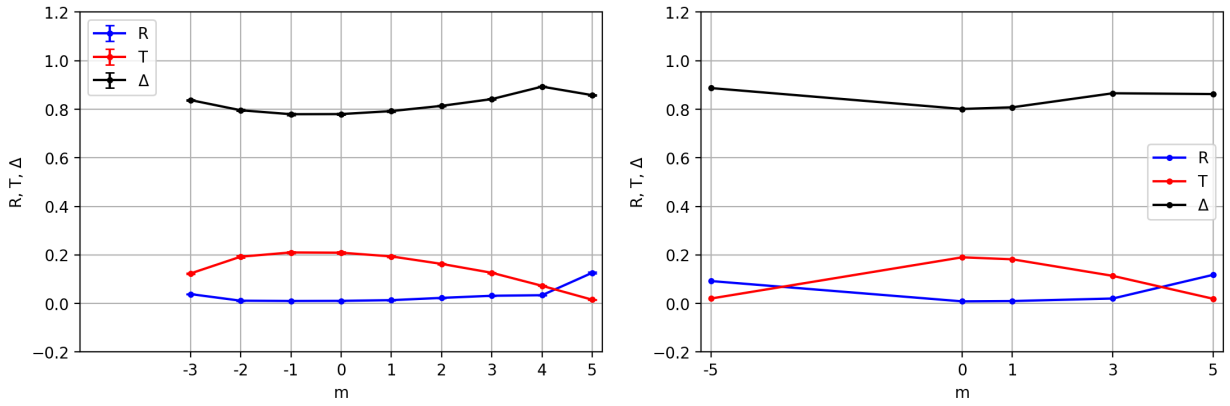

Fig. 15 Scattering Coefficients R, T, Δ for liner measurements and different modes excited at 1500Hz. Left:LSF, right: BOMP.

V. Conclusion and Future Work

With the mode synthesizer (MOSY) setup we have established a new facility with appropriate test and measurement procedures for the more realistic investigation of liner structures. The annular duct with outer diameter of 500 mm enables the investigation of homogeneous, locally reacting, and non-locally reacting liner structures in various ratios of length to diameter. With the current setup, azimuthal modes $m = -8...8$ and radial mode orders $n = 0$ and $n = 1$ can be excited with a significant suppression of all other modes. Usually, the next highest mode has an amplitude which is 10 dB or more below the excited mode. Care must be taken by the selection of the test frequencies with certain frequency ranges being densely populated by cut-on frequencies of various modes - which represents a serious challenge for the accurate measurement of the mode under observation or/and the respective excitation. Two different algorithms for the radial mode analysis have been applied, namely the LSF and the BOMP algorithm. While the first one is expected to be limited by the amplification of disturbances beyond approximately 2000 Hz in the current setup, the BOMP showed good results up to about 3500 Hz with limitations only in the region of many cut-on modes (here around 2000-2400 Hz).

A first test case, using a foam patch showed exemplary measurement capabilities for this test rig. The increased damping of higher order modes can be precisely measured and will yield the possibility to validate respective attenuation models which are needed to estimate the liner performance for wide ducts with many modes being cut-on.

Further, the viscothermal losses within the acoustic boundary layer could be measured using a hardwall section and compared to a model by Weng [15]. They are found to be very small for the current setup, but might increase for longer test objects or with flow, which can be also accounted for by this model.

Future work will include a more in-depth analysis of the acquired data, which includes also test cases with flow (positive and negative direction compared to acoustic propagation), the extension of the analysis to broadband white noise measurements and most important other liner structures. With the very good measurement accuracy, it will be possible to investigate also non-uniform structures with variations over the circumference (e.g. non-locally reacting liners and splices) which are expected to generate spill over from the excited modes into other mode orders.

Acknowledgements

This work was partially funded within the framework of the LuFo VI-1 project “FLIER“ (Flexible wall structures for acoustic Liners, contract number 20E1915B) and the LuFo VI-1 project “MUTE“ (Methoden und Technologien zur Vorhersage und Minderung von Triebwerkslärm) by the Federal Ministry for Economic Affairs and Climate Action based on a decision of the German Bundestag, which is gratefully acknowledged. Further support was obtained from DLR-internal project “SIAM”.

The trademark Basotect® - which is used in some instances throughout the text/graphs for reasons of simplification cases without the proper trademark sign - is owned by the company BASF.

The authors want to thank the DLR workshop team (Angelo Rudolphi, Sebatian Kruck, and Sven Nieländer) for their support in the setup and manufacturing of the liner barrel, and Ralf Burgmayer and further colleagues of the DLR engine acoustics department for various support activities during the tests and associated data processing.

References

[1] Gerhold, C. H., Brown, M. C., Watson, W. R., and Jones, M. G., "Investigation of liner characteristics in the NASA Langley curved duct test rig," *13th AIAA/CEAS Aeroacoustics Conference, 21-23 May 2007, Rome, Italy*, 2007. AIAA-2007-3532.

[2] Gerhold, C. H., Brown, M. C., Jones, M. G., and Howerton, B. M., "Analysis of liner performance using the NASA Langley Research Center Curved Duct Test Rig," *Applied Acoustics*, Vol. 102, 2016, pp. 19–32. https://doi.org/https://doi.org/10.1016/j.apacoust.2015.07.006, URL https://www.sciencedirect.com/science/article/pii/S0003682X15001991.

[3] Humbert, T., Golliard, J., Portier, E., Gabard, G., and Auregan, Y., "Multimodal characterisation of acoustic liners using the MAINE Flow facility," *28th AIAA/CEAS Aeroacoustics Conference, 14-17 June 2022, Southampton, UK*, 2022. https://doi.org/10.2514/6.2022-3082.

[4] Sitel, A., Ville, J.-M., and Foucart, F., "An Experimental Facility for Measurement of Acoustic Transmission Matrix and Acoustic Power Dissipation of Duct Discontinuity in Higher Order Modes Propagation Conditions," *Acta Acustica united with Acustica*, Vol. 89, No. 4, 2003, pp. 586–594.

[5] Tapken, U., and Enghardt, L., "Optimisation of Sensor Arrays for Radial Mode Analysis in Flow Ducts," *12th AIAA/CEAS Aeroacoustics Conference*, Cambridge, Massachusetts (USA), 2006. https://doi.org/10.2514/6.2006-2638.

[6] Tapken, U., and Nagai, K., "Effects Impairing the Synthesis of Acoustic Duct Modes with Loudspeaker Arrays," *19th International Congress on Sound and Vibration*, Vilnius, Lithuania, 2012.

[7] Tapken, U., "Analyse und Synthese akustischer Interaktionsmoden von Turbomaschinen," Dissertation, Technische Universität Berlin, Berlin, Deutschland, 2016. https://doi.org/10.14279/depositonce-5124.

[8] Gensch, T., and Tapken, U., "Comparison of different approaches to the selective synthesis of dominant duct modes in turbomachines using loudspeakers," *27th International Congress on Sound and Vibration - ICSV27*, Prague, Czech Republic, 2021.

[9] Behn, M., Klähn, L., and Tapken, U., "Comprehensive experimental investigation of mode transmission through stator vane rows: Results and calibration of an analytical prediction model," *23rd AIAA/CEAS Aeroacoustics Conference*, Denver, Colorado (USA), 2017. https://doi.org/10.2514/6.2017-3218.

[10] Seiner, J., and Reethof, G., "Design and development of the spinning mode synthesizer," Contractor Report NASA-CR-2260, Pennsylvania State University and NASA, 4 1973. URL https://ntrs.nasa.gov/search.jsp?R=19730012340.

[11] Johnson, M., and Fuller, C., "Development and Testing of a High Level Axial Array Duct Sound Source for the NASA Flow Impedance Test Facility," Contractor Report NASA/CR-2000-210645, Fuller Technologies, Inc.; NASA, 2000. URL https://ntrs.nasa.gov/search.jsp?R=20010019757.

[12] Snakowska, A., Gorazd, L., Jurkiewicz, J., and Kolber, K., "Generation of a single cylindrical duct mode using a mode synthesiser," *Applied Acoustics*, Vol. **114**, 2016, pp. 56 – 70. https://doi.org/10.1016/j.apacoust.2016.07.007.

[13] Eldar, Y. C., "Block-Sparse Signals: Uncertainty Relations and Efficient Recovery," *IEEE Transactions on Signal Processing*, Vol. 58, No. 6, 2010, pp. 3042–3054.

[14] Hurst, J., Behn, M., Tapken, U., and Enghardt, L., "Sound Power Measurements at Radial Compressors Using Compressed Sensing Based Signal Processing Methods," 2019. https://doi.org/10.1115/GT2019-90782.

[15] Weng, C., and Bake, F., "An analytical model for boundary layer attenuation of acoustic modes in rigid circular ducts with uniform flow," *Acta Acoustica United with Acoustica*, Vol. 102, 2016, pp. 1138–1141. Short Communications.

[16] Weng, C., Schulz, A., Ronneberger, D., Enghardt, L., and Bake, F., "Flow and viscous effects on impedance eduction," *AIAA Journal*, Vol. 56, No. 3, 2018, pp. 1118–1132. https://doi.org/10.2514/1.J055838.

[17] Kirchhoff, G., "Über den Einfluss der Wärmeleitung in einem Gase auf die Schallbewegung," *Annalen der Physik und Chemie*, Vol. 210, No. 6, 1868, pp. 177–193. https://doi.org/10.1002/andp.18682100602.

[18] Beatty, R. E., "Boundary layer attenuation of higher order modes in rectengular and circular tubes," *Journal of the Acoustical Society of America*, Vol. 22, No. 6, 1950, pp. 850–854.

[19] Rice, E., and Heidmann, M., "Modal propagation angles in a cylindrical duct with flow and their relation to sound propagation." *Proceedings of the 17th Aerospace Science Meeting*, New Orleans, USA, 1979.

[20] Heidelberg, L., Rice, E., and Homyak, L., "Acoustic performance of inlet suppressors on an engine generating a single mode," *7th Aeroacoustics Conference*, 1981. https://doi.org/10.2514/6.1981-1965, URL https://arc.aiaa.org/doi/abs/10.2514/6.1981-1965.